Comparison of Semiconducting Polymer Dots and Semiconductor Quantum Dots for Smartphone-Based Fluorescence Assays

Rupsa Gupta[1], William J. Peveler[1,2], Kelsi Lix[1], W. Russ Algar[1]*.

[1] Department of Chemistry, University of British Columbia, 2036 Main Mall, Vancouver, British Columbia, V6T 1Z1, Canada.

[2] School of Chemistry, Joseph Black Building, University of Glasgow, Glasgow, G12 8QQ, U.K.

ABSTRACT: Fluorescent nanoparticles have transformative potential for smartphone-based point-of-need diagnostics because an optimal material can reduce the technical burden to meet assay performance requirements. Semiconductor quantum dots (QDs) are a now well-established example of such a material. Semiconducting polymer dots (Pdots) and conjugated-polymer nanoparticles (CPNs) are emerging materials that bring advantages of brightness, synthetic ease, and being metal-free versus QDs, but frequently present the trade-off of spectrally broad emission and less well-defined surface chemistry. Here, we compare these two classes of nanoparticle in the context of a "bare bones" device that uses the smartphone for all-in-one excitation and imaging of fluorescence. The greater per-particle brightness of Pdots provides orders of magnitude better imaging sensitivity versus QDs, and this advantage translates to a model lateral flow assay. Our data suggests that Pdots will support multicolor imaging on a smartphone in an optimized assay, although QDs are likely superior for this purpose. These pros and cons lead to discussion of how physicochemical differences between QDs and Pdots may influence assay performance beyond differences in optical properties. Overall, Pdots have great potential for enabling smartphone-based fluorescence assays with high sensitivity and low detection limits.

INTRODUCTION

The development of smartphone-based imaging and assays has been driven by the need for inexpensive and robust biomedical diagnostic tools that can operate in remote or low-resource settings.[1] The combination of a camera, onboard processor, and network connectivity has been widely exploited to image lateral flow assays,[2] paper-based ELISAs,[3] well plates,[4] and other colorimetric and fluorometric assays.[5,6,7] Particular attention has been given to the engineering of such systems, working with 3D-printed peripherals,[8,9] elegant optical stacks,[10] and incorporation of LEDs, lasers, and other optoelectronics to optimize assay performance.[11] The assays themselves are typically designed around tried-and-tested colorimetric and fluorometric methods and materials, such as gold nanoparticles[12] and small molecule dyes.[13]

In the case of fluorometric assays, the broad absorption spectra, narrow emission spectra, high brightness, and large effective Stokes shifts of semiconductor quantum dots (QDs) have been shown to be particularly well suited to smartphone imaging.[11] The hard, core-shell structure and scope of well-developed surface chemistries also make QDs attractive for the preparation of bioconjugates.[14] Forgoing the peripheral LEDs and lasers commonly used, we have previously shown that QDs paired with a simple combination of filters and a smartphone flash and camera will yield excellent results in binding and proteolytic assays, including decisive advantages over fluorescent dyes.[7] This "bare-bones" approach lends itself well to the sought after low-cost, reproducible, and robust diagnostic tools. The QDs, as a materials-led innovation, are an alternative to making reader-technologies more sophisticated in order to obtain similar performance with less-ideal fluorophores.

New functional fluorescent materials are emerging that may be able to go beyond the advantages that QDs offer over dyes. One such class of materials is conjugated-polymer nanoparticles (CPNs), of which semiconducting polymer dots (Pdots) are a subset. Pdots have a diameter < 30 nm, > 50% π-conjugated semiconducting polymer (by mass or volume), and a hydrophobic core.[15] The dense packing of multiple conjugated chromophore units inside a Pdot results in very large absorption cross-sections that increase with particle size. The color of fluorescence is tuned by selection of the semiconducting polymer rather than by the size of the particle. Surface functionality is introduced either by incorporating reactive groups into the backbone of the semiconducting polymer itself,[16,17] or, more commonly, by co-precipitation of the semiconducting polymer with amphiphilic stabilizing agents that have handles for further chemical modification.[18,19]

Since their introduction in 2005,[20] Pdots have been increasingly adopted for biological assays and sensors,[15] where their high brightness has led to very promising sensitivities and detection limits,[21] including with smartphones.[22] One challenge that many Pdot materials bring with them is their broad emission spectra, which is less ideal for multiplexed detection than the spectrally-narrow emission from QDs, albeit that strategies have been developed for addressing this limitation.[23,24]

Here, we evaluate Pdots as an alternative fluorophore in "bare-bones" smartphone-based assays, using QDs as a gold-standard material for comparison. We show that the superior brightness of Pdots versus QDs translates into more sensitive detection on a smartphone, including a lower detection limit in a model assay. Our data also suggest that QDs are more optimal for multicolor measurements via smartphone imaging, although Pdots do show

potential for this capability. Other considerations in comparing QDs and Pdots are also discussed. Overall, Pdots hold significant promise for materials-led enablement and optimization of smartphone-based bioanalyses and imaging. For applications requiring maximum brightness, Pdots and CPNs are likely a better material than QDs.

EXPERIMENTAL METHODS

Additional details for the materials and methods can be found in the Supporting Information (SI).

Pdots were synthesized by co-precipitation of fluorescent polymer, poly(9,9-dioctylfluorene-*alt*-benzothiadiazole) (F8BT; M_n 17–23 kDa) or cyano-polyphenylene vinylene (CNPPV; M_w 350 kDa), with a poly(styrene)-poly(ethylene glycol) (PS-PEG; M_n 36.5 kDa) or poly(styrene-*co*-maleic anhydride) (PSMA; M_n 1.7 kDa) amphiphilic polymer, using a modification of the method from the group of Chiu.[25] Concentrations were determined by nanoparticle tracking analysis (NTA).

CdSeS/ZnS QDs were from CytoDagnostics (Burlington, ON, Canada) and CdSe/CdS/ZnS QDs were synthesized by the decomposition of inorganic precursors in organic solvents during hot injection.[26,27] QDs were coated with glutathione ligands (GSH) or encapsulated with poly(maleic anhydride-*alt*-1-octadecene) (PMAO) polymer via an adapted phase exchange procedure.[28] Concentrations were estimated from absorption spectra.[29] Table S1 lists which materials were used for which experiments.

PS-PEG-coated Pdots and the PMAO-coated QDs were conjugated with goat IgG using carbodiimide/succinimidyl ester chemistry, with purification by centrifugal filtration.

The smartphone apparatus was analogous to one we reported previously,[7] excepting modification to fit a Samsung Galaxy S7 smartphone. Spectrofluorimetric and absorbance measurements were made with an Infinite M1000 multifunction plate reader (Tecan, Morrisville, NC). Excitation parameters were approximately matched between the plate reader and smartphone apparatus (*vide infra*).

RESULTS AND DISCUSSION

Particle comparison. The polymer nanoparticles that we prepared are larger than typical Pdots; however, we refer to these materials as Pdots because of their high brightness and high percentage of semiconducting polymer. Figure 1A-B illustrates the structural differences between the Pdots and QDs, and compares their sizes. Figures 1C-D show representative size characterization data for the Pdots. For the F8BT and CNPPV Pdots, the respective mean sizes from transmission electron microscopy (TEM) were 57 ± 16 nm (N = 101, mode = 52 nm) and 43± 7 nm (N = 101, mode = 40 nm), and, from NTA were, 66 ± 37 nm (N = 4697, mode = 54 nm) and 62 ± 37 nm (N = 576, mode = 56 nm). The mean TEM sizes of the QD540a and QD630 cores were 6.0 ± 1.2 nm (N = 468, mode = 5.8 nm) and 9.1 ± 1.5 nm (N = 575, mode = 8.6 nm), respectively. Hydrodynamic diameters of the corresponding PMAO-coated QDs were 11 ± 2 nm and 13 ± 5 nm. Additional characterization data for the QDs can be found in the SI.

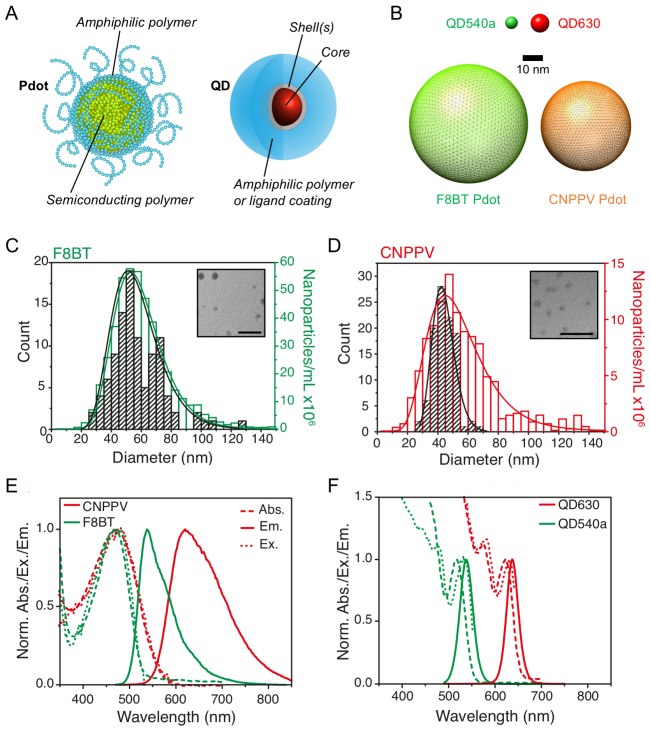

Figure 1. (A) Cartoon illustrations of a Pdot and QD. (B) Size comparison between the Pdots and QDs. Size of (C) F8BT Pdots and (D) CNPPV Pdots by TEM (left axis) and NTA (right axis, color). All fitted curves are lognormal distributions. Scale bars are 200 nm for the inset TEM images. Normalized absorption (dashed line), PL excitation (dotted line), and emission spectra (solid line) for the (E) Pdots and (F) QDs.

Figures 1E-F compare the absorption and photoluminescence (PL) excitation and emission spectra for the F8BT and CNPPV Pdots with those of a CdSeS/ZnS QD (QD540a) and a CdSe/CdS/ZnS QD (QD630). To the naked eye, the QD540a, F8BT Pdots, CNPPV Pdots, and QD630 luminesced green, green-yellow, orange, and red, respectively. The Pdot materials had an absorption/excitation maximum at *ca.* 450 nm. PL emission was spectrally asymmetric with peaks at 538 nm and 620 nm for F8BT and CNPPV, respectively, and full-widths-at-half-maximum (FWHM) of 76 nm and 130 nm. The QD540a and QD630 had symmetric PL emission spectra with maxima at 540 nm and 630 nm, respectively, and FWHMs of 32 nm and 29 nm. The absorption spectra of the QDs exhibited characteristic increases from the first exciton peaks (518 nm and 622 nm) into the UV region.

Brightness, B, per Eqn. 1, is the product of molar absorption coefficient at the excitation wavelength, $\varepsilon(\lambda)$, and the PL quantum yield, Φ. It is the main non-technical determinant of sensitivity in most fluorescence experiments.

$$B(\lambda) = \varepsilon(\lambda)\Phi \qquad (1)$$

The brightness of the QDs and Pdots at an excitation wavelength of 450 nm is compared in Table 1. Given the quantum yields of both materials (Figure S5), the molar absorption coefficient is the major contributing factor to the hugely superior brightness of Pdots over QDs.

Table 1: Approximate molar extinction coefficients and brightness values for Pdots and QDs at 450 nm excitation.

Particle	ε_{450} (10^5 M^{-1} cm^{-1}) [a]	Φ [b]	B_{450} (10^5 M^{-1} cm^{-1}) [c]
QD630	23	0.44 ± 0.10	9 ± 2
QD540a	3.6	0.58 ± 0.10	1.7 ± 0.3
CNPPV Pdot	41 (± 26) × 10^3	0.37 ± 0.3	15 (± 10) × 10^3
F8BT Pdot	33 (± 30) × 10^3	0.35 ± 0.24	12 (± 10) × 10^3

Notes: [a] Estimated molar extinction coefficient at 450 nm; [b] quantum yield; [c] Brightness at 450 nm. Uncertainties for Pdots (PSMA amphiphile) are largely batch-to-batch variation (average size 54 nm for F8BT, 50 nm for CNPPV). Uncertainties for QDs (GSH-coated) are measurement imprecision for a single batch of material.

One-color measurements. Figure 2A compares PL intensities versus concentration for the QDs and Pdots from spectrofluorimetric measurements and from smartphone imaging. In both cases, picomolar concentrations of Pdots produced intensities similar to those from nanomolar concentrations of QDs. Figure 2B shows representative smartphone images.

Figure 2C is a schematic of the smartphone apparatus. Light from the camera flash was filtered to select blue wavelengths (centered at 447 nm), reflected onto the sample, and sample PL imaged by the camera through a filter that transmitted green through red light (> 500 nm). This apparatus was designed for a Galaxy S7 phone, but also accommodated the S8 model and is adaptable to other camera models.[7] The smartphone-based measurement differed from a spectrofluorimetric measurement in the bandwidth of excitation, wavelength selection mechanism, and detector sensitivity. These differences are elaborated on in the SI; however, to make the PL measurements on the spectrofluorimeter more comparable to those on the smartphone, the spectrofluorimetric PL intensities were integrated over the estimated wavelength ranges of the red and green channels of the smartphone camera (580–700 nm and 500–620 nm for the red- and green-emitting materials, respectively). The similarity of the data between the spectrofluorimeter and smartphone imaging clearly indicated that the brightness advantage of the Pdots translated between the two disparate measurement formats.

Two-color measurements. For multicolor imaging, the spectrally broad PL of the Pdots is less ideal than the spectrally narrow PL of QDs, which have previously enabled three-color imaging via the built-in RGB filters and channels of a smartphone camera.[6] We therefore evaluated whether crosstalk correction could enable two-color measurements with F8BT and CNPPV Pdots via the red (R) and green (G) channels of smartphone images. QD540a and QD630 were also assessed for comparison. Measurements were made with mixtures of QDs or Pdots in bulk solution and spotted onto a nitrocellulose membrane.

To determine crosstalk correction factors, samples of exclusively green-luminescent material (F8BT, QD540a) or red-luminescent material (CNPPV, QD630) were measured. The recorded intensities in the R and G channels of smartphone images (I_G and I_R) of a single color of nanoparticle were substituted into eqns. 2 & 3, where S_G and S_R are the corrected PL emission signals for the green- and red-luminescent materials, and σ_R and σ_G are the crosstalk correction factors for the signal from those materials in the non-nominal color channel.

$$I_G = S_G + \sigma_G S_R \quad (2)$$

$$I_R = \sigma_R S_G + S_R \quad (3)$$

In the case of mixtures with different amounts of the green- and red-luminescent materials, eqns. 2 & 3 were solved simultaneously to find the signals for each material.

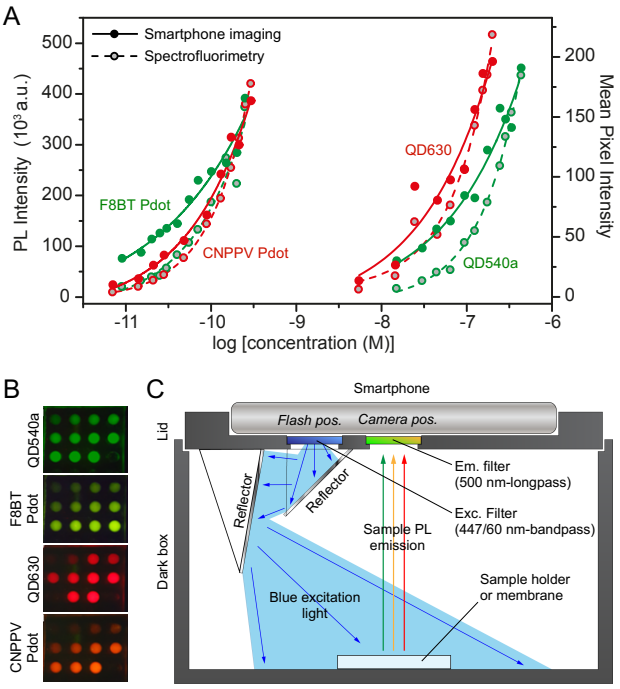

Figure 2. (A) PL intensity versus concentration for Pdots and QDs via spectrofluorimetry and via smartphone imaging. (B) Representative smartphone PL images. (C) Schematic of the apparatus for smartphone imaging.

For both solution-phase and spotted-on-membrane mixtures, Figure 3 shows plots of the calculated green/red material signal ratios (S_G/S_R) measured by smartphone imaging versus the same ratios measured by spectrofluorimetry (g/r). The spectrofluorimetric signals for a mixture of Pdots or QDs were unmixed as a linear combination of the corresponding PL emission spectra (see SI for details). As this process is very reliable, the ideal results for the plots in Figure 3 are straight lines with minimal deviations of the data points from the line (*i.e.* small root mean square error (RMSE)). The slopes will not be unity because the camera color sensitivity differs from that of the spectrofluorimeter.

In solution, the line for the QDs had a slope of 0.67 with a RMSE of 0.10 (relative RMSE 15%); the line for the Pdots had a slope of 0.82 with a similar RMSE of 0.14 (relative RMSE 16%). On a membrane, there was a larger difference between the Pdots and QDs. The QDs had a slope of 0.98 with a RMSE of 0.08 (relative RMSE 9%), whereas the Pdots had a slope of 0.61 and a less favorable RMSE of 0.23 (relative RMSE 38%).

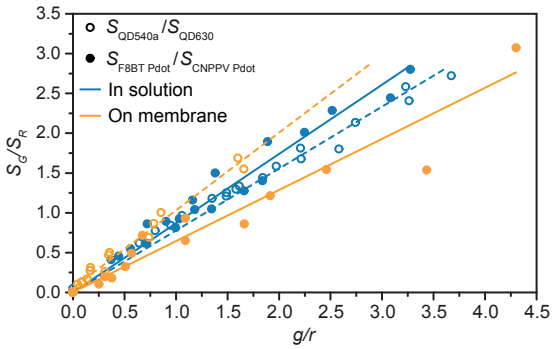

Figure 3. Green-to-red signal ratio from mixtures of Pdots and QDs measured via smartphone imaging versus on a spectrofluorimetry. Data is shown for a mixture in bulk solution (GSH-QDs, PSMA-Pdots) and a mixture spotted on a nitrocellulose membrane (PMAO-QDs, PS-PEG-Pdots).

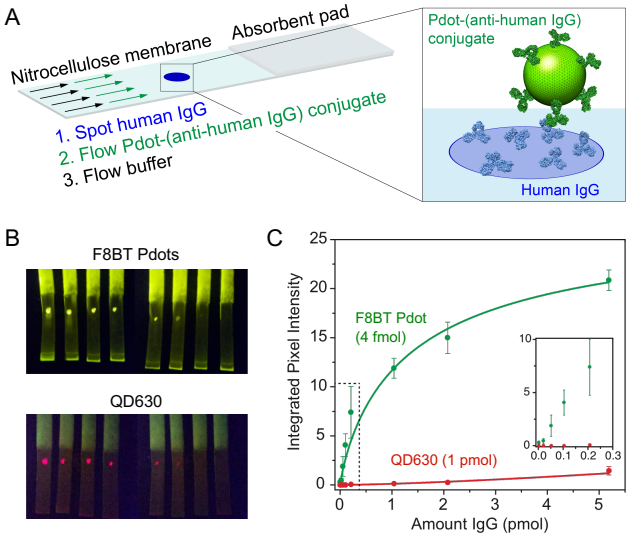

Figure 4. (A) Cartoon illustration of the model lateral flow-like assay for human IgG. F8BT Pdots and QD630, each conjugated with goat-anti-human IgG, were compared. Analyte spots contained between 2 fmol and 5 pmol of human IgG. (B) Representative smartphone PL images (ISO 400, shutter speed 1/6 s) of the membranes. The brightness of the QD image was digitally enhanced for clarity (see Figure S12 for original). (C) Dose-response curve for the assays. Error bars are standard deviations on three independent replicate experiments. The dotted-line region is shown in the inset.

Model assay. To further compare Pdots and QDs for smartphone imaging, a model binding assay was carried out in a format resembling a paper test strip or lateral flow assay. The target analyte was human IgG, and the QDs or Pdots were modified with goat anti-human-IgG antibodies via carbodiimide coupling. Conjugation was confirmed by agarose gel electrophoresis (Figure S10). The ratio of antibody to nanoparticle was adjusted for each material to aim for maximal surface coverage (using a small excess) without crosslinking the antibodies and particles. It was estimated, based on nanoparticle radii and a minimal footprint of 38 nm^2 per IgG,[30] that Pdots accommodated approximately 20–40 times as many antibodies as QDs.

Human IgG analyte was spotted onto nitrocellulose membranes at different concentrations. The antibody-conjugated F8BT Pdots and QD630 were flowed (by capillary action) over the dried spots of analyte and bound to the target, as illustrated in Figure 4A. These nanoparticles were selected as the brightest of each type of material under smartphone imaging (Fig. 2A). As expected, higher binding was observed as higher PL intensities at higher target concentrations. Despite the use of 250-times more QDs than Pdots in the assays (to account for both the inherent differences in antibody-per-particle and brightness), the Pdots were an order of magnitude more intense under the same imaging conditions, greatly improving sensitivity. Figures 4B-C show representative smartphone images and the dose-response curves for the model assays. The Pdots were detected at >20 fmol of human IgG, whereas the QDs were only detected at >100 fmol, with much lower signal intensity from a greater concentration of particles used.

DISCUSSION AND CONCLUSIONS

The brightness of Pdots is key to their appeal for incorporation into bioassays. This brightness results from the multiple polymer chains incorporated into the core of the Pdot, each representing multiple chromophoric sites. In contrast, QDs are single chromophores with much smaller net absorption cross-sections. Our data shows that both materials are bright enough to image using only flash excitation, but the more efficient absorption of excitation light by the Pdots results in lower detection limits. Use of excitation wavelengths better optimized to the QDs (e.g. violet light offers ~2-fold better excitation of QDs and ~3-fold less efficient excitation of Pdots) would not significantly change the results because of the approximate 1000-fold difference in brightness. The brightness advantage of Pdots is thus emphasized by our bare-bones smartphone apparatus, but not limited to its technical specifications, consistent with other head-to-head comparisons of QDs and Pdots with sophisticated instruments.[28]

The potential drawback for Pdots is their much broader emission. Our results with mixtures of Pdots in bulk solution suggest that Pdots can be competitive with QDs for red/green assays on a smartphone when using a simple mathematical correction for crosstalk. In contrast, our membrane results suggest an advantage for QDs. We speculate that the discrepancy between these two formats came from solid-phase effects such as coffee ringing, particle aggregation (with potential for green-to-red energy transfer), and potential surface-induced unfolding or restructuring of Pdots on the membrane. We anticipate that optimization of the assay format and particle chemistry (for greater

stability) will remedy this shortcoming. Certainly, the brightness advantage warrants further exploration of multicolor Pdot-assay formats on a smartphone. Three-color measurements with Pdots, similar to those we have done with QDs,[6] would be more challenging than two-color measurements, but far from impossible. Re-engineering semiconducting polymers (e.g. incorporation of BODIPY units) for more narrow emission FWHMs is potential route to three-color capability.[31,24]

Besides brightness and emission FHWM, there are other non-trivial differences between QDs and Pdots. Although smaller Pdots (*ca.* 20 nm) can be prepared,[32] Pdots and CPNs will generally be larger and more polydisperse than QDs. Different maximum densities of nanoparticle on an interface (*e.g.* membrane) are therefore expected, which may influence assay dynamic range. The nanoparticle surface area available for non-specific binding may also differ and affect assay selectivity, with a potential role for the hard versus soft nature of QDs and Pdots in determining the mechanism(s) of non-specific binding. Differences in the maximum number of antibodies per nanoparticle may also impact the statistics and avidity of binding, including the likelihood that, for poorly-controlled conjugation chemistries (*e.g.* carbodiimide), each NP has antibodies conjugated in an optimal orientation for target binding.

Other practical differences in assay development arise from the contrasting synthetic and materials properties between Pdots and QDs. A potential drawback of QDs is that, presently, the best and brightest materials incorporate heavy metals such as cadmium. The amounts of cadmium per assay are sub-microgram (less than the permissible daily intake of 0.8 μg/kg bodyweight[33]), but still preferable to avoid for regulatory and disposal reasons. Although heavy-metal-free QDs are in development, these materials currently have lower brightness and wider PL emission FWHM. Pdots thus come to the fore as an attractive metal-free alternative. Pdots also have the advantage of being synthesized in one step in a ready-to-functionalize form in aqueous solution, whereas the preparation of high-quality aqueous QDs is an intensive, multi-step process. Nevertheless, in our hands, we found that the synthetic ease of Pdots came at a cost of reduced shelf-life and more fickle colloidal stability versus QDs. Storage and conjugation reaction conditions needed to be finely tuned to avoid adverse effects on the Pdots (*e.g.* aggregation, adhesion to reaction vessels). These challenges were, at one time, also common with QDs, so we expect that further development of Pdot surface and bioconjugate chemistry will overcome these limitations. Several strategies can be adapted from other materials,[34,14] and new methods that leverage the unique Pdot surface chemistry are already being implemented.[35]

Another caveat with respect to Pdots, in our hands, is significant inter-batch variability, which accounts for the large uncertainties in Table 1 (e.g. CNPPV Pdots were brightest on average, but F8BT Pdots were brighter for the batches used for Figures 1-4.) In contrast, we achieve better (but not perfect) inter-batch consistency with QDs, likely in part from a more direct relationship between optical properties and size. Uncertainties in the concentrations of Pdots and QDs also contribute to the uncertainties in Table 1. For QDs, the maximum uncertainty is approximately a factor of two, which arises from the choice of model for their molar absorption coefficient.[29,36,37] For Pdots, concentrations (and thus molar extinction coefficients) were measured via NTA (and absorbance). We estimate the typical accuracy to be within a factor of three, and, at worst, accurate within an order of magnitude. This uncertainty is currently secondary to the batch-to-batch variation, but will eventually need to be considered for reproducible optimization of the number of antibodies per Pdot. Even so, this uncertainty does not alter the conclusion that the Pdots were orders of magnitude brighter than the QDs.

In summary, the selection between QDs and Pdots for smartphone-based assays is a multifaceted problem. The brightness advantage we demonstrated for Pdots translates into orders-of-magnitude better sensitivity and lower detection limits. However, overall superior performance in an assay—which also considers selectivity, multiplexing, and other requirements—may warrant engineering and optimization of Pdots with respect to their particle chemistry and emission properties. Nevertheless, Pdots have great potential for smartphone-based fluorescence assays.

ASSOCIATED CONTENT

Supporting Information

The Supporting Information are available free of charge on the ACS Publications website.

Experimental methods, additional data (PDF)

AUTHOR INFORMATION

Corresponding Author

* Prof. W.R Algar, algar@chem.ubc.ca

ACKNOWLEDGMENT

We thank NSERC, CFI, BCKDF, and UBC for support of this research. R.G. is grateful for support through the NSERC CREATE NanoMat training program. W.J.P. gratefully acknowledges the Izaak Walton Killam Memorial Fund for Advanced Studies for a Postdoctoral Fellowship, and the University of Glasgow for a Lord Kelvin Adam Smith Fellowship. W.R.A. is grateful for a Canada Research Chair, a Michael Smith Foundation for Health Research Scholar Award, and an Alfred P. Sloan Research Fellowship.

REFERENCES

(1) Hernández-Neuta, I.; Neumann, F.; Brightmeyer, J.; Ba Tis, T.; Madaboosi, N.; Wei, Q.; Ozcan, A.; Nilsson, M. Smartphone-based Clinical Diagnostics: Towards Democratization of Evidence-based Health Care. *J. Intern. Med.* **2019**, *285*, 19–39.

(2) Brangel, P.; Sobarzo, A.; Parolo, C.; Miller, B. S.; Howes, P. D.; Gelkop, S.; Lutwama, J. J.; Dye, J. M.; McKendry, R. A.; Lobel, L. A Serological Point-of-Care Test for the Detection of IgG Antibodies against Ebola Virus in Human Survivors. *ACS Nano* **2018**, *12*, 63–73.

(3) Murdock, R. C.; Shen, L.; Griffin, D. K.; Kelley-Loughnane, N.; Papautsky, I.; Hagen, J. A. Optimization of a Paper-Based ELISA for a Human Performance Biomarker. *Anal. Chem.* **2013**, *85*, 11634–11642.

(4) Kim, D.; Wei, Q.; Kim, D. H.; Tseng, D.; Zhang, J.; Pan, E.; Garner, O.; Ozcan, A.; Di Carlo, D. Enzyme-Free Nucleic Acid Amplification Assay Using a Cellphone-Based Well Plate Fluorescence Reader. *Anal. Chem.* **2018**, *90*, 690–695.

(5) Oncescu, V.; O'Dell, D.; Erickson, D. Smartphone Based Health Accessory for Colorimetric Detection of Biomarkers in Sweat and Saliva. *Lab Chip* **2013**, *13*, 3232.

(6) Petryayeva, E.; Algar, W. R. Multiplexed Homogeneous Assays of Proteolytic Activity Using a Smartphone and Quantum Dots. *Anal. Chem.* **2014**, *86*, 3195–3202.

(7) Petryayeva, E.; Algar, W. R. A Job for Quantum Dots: Use of a Smartphone and 3D-Printed Accessory for All-in-One Excitation and Imaging of Photoluminescence. *Anal. Bioanal. Chem.* **2016**, *408*, 2913–2925.

(8) Knowlton, S.; Joshi, A.; Syrrist, P.; Coskun, A. F.; Tasoglu, S. 3D-Printed Smartphone-Based Point of Care Tool for Fluorescence-and Magnetophoresis-Based Cytometry. *Lab Chip* **2017**, *17*, 2839–2851.

(9) Kanakasabapathy, M. K.; Pandya, H. J.; Draz, M. S.; Chug, M. K.; Sadasivam, M.; Kumar, S.; Etemad, B.; Yogesh, V.; Safavieh, M.; Asghar, W. Rapid, Label-Free CD4 Testing Using a Smartphone Compatible Device. *Lab Chip* **2017**, *17*, 2910–2919.

(10) Wei, Q.; Qi, H.; Luo, W.; Tseng, D.; Ki, S. J.; Wan, Z.; Göröcs, Z.; Bentolila, L. A.; Wu, T. T.; Sun, R.; et al. Fluorescent Imaging of Single Nanoparticles and Viruses on a Smart Phone. *ACS Nano* **2013**, *7*, 9147–9155.

(11) Petryayeva, E.; Algar, W. R. Toward Point-of-Care Diagnostics with Consumer Electronic Devices: The Expanding Role of Nanoparticles. *RSC Adv.* **2015**, *5*, 22256–22282.

(12) Lee, S.; Oncescu, V.; Mancuso, M.; Mehta, S.; Erickson, D. A Smartphone Platform for the Quantification of Vitamin D Levels. *Lab Chip* **2014**, *14*, 1437–1442.

(13) Priye, A.; Bird, S. W.; Light, Y. K.; Ball, C. S.; Negrete, O. A.; Meagher, R. J. A Smartphone-Based Diagnostic Platform for Rapid Detection of Zika, Chikungunya, and Dengue Viruses. *Sci. Rep.* **2017**, *7*, 44778.

(14) Sapsford, K. E.; Algar, W. R.; Berti, L.; Gemmill, K. B.; Casey, B. J.; Oh, E.; Stewart, M. H.; Medintz, I. L. Functionalizing Nanoparticles with Biological Molecules: Developing Chemistries That Facilitate Nanotechnology. *Chem. Rev.* **2013**, *113*, 1904–2074.

(15) Yu, J.; Rong, Y.; Kuo, C.-T.; Zhou, X.-H.; Chiu, D. T. Recent Advances in the Development of Highly Luminescent Semiconducting Polymer Dots and Nanoparticles for Biological Imaging and Medicine. *Anal. Chem.* **2016**, *89*, 42–56.

(16) Zhang, X.; Yu, J.; Wu, C.; Jin, Y.; Rong, Y.; Ye, F.; Chiu, D. T. Importance of Having Low-Density Functional Groups for Generating High-Performance Semiconducting Polymer Dots. *ACS Nano* **2012**, *6*, 5429–5439.

(17) Xie, C.; Zhen, X.; Lei, Q.; Ni, R.; Pu, K. Self-Assembly of Semiconducting Polymer Amphiphiles for In Vivo Photoacoustic Imaging. *Adv. Funct. Mater.* **2017**, *27*, 1605397.

(18) Wu, C.; Bull, B.; Szymanski, C.; Christensen, K.; McNeill, J. Multicolor Conjugated Polymer Dots for Biological Fluorescence Imaging. *ACS Nano* **2008**, *2*, 2415–2423.

(19) Wu, C.; Schneider, T.; Zeigler, M.; Yu, J.; Schiro, P. G.; Burnham, D. R.; McNeill, J. D.; Chiu, D. T. Bioconjugation of Ultrabright Semiconducting Polymer Dots for Specific Cellular Targeting. *J. Am. Chem. Soc.* **2010**, *132*, 15410–15417.

(20) Szymanski, C.; Wu, C.; Hooper, J.; Salazar, M. A.; Perdomo, A.; Dukes, A.; McNeill, J. Single Molecule Nanoparticles of the Conjugated Polymer MEH-PPV, Preparation and Characterization by near-Field Scanning Optical Microscopy. *J. Phys. Chem. B* **2005**, *109*, 8543–8546.

(21) Fang, C.-C.; Chou, C.-C.; Yang, Y.-Q.; Wei-Kai, T.; Wang, Y.-T.; Chan, Y.-H. Multiplexed Detection of Tumor Markers with Multicolor Polymer Dot-Based Immunochromatography Test Strip. *Anal. Chem.* **2018**, *90*, 2134–2140.

(22) Yuan, Z.; Zhang, X.; Wu, C. Ultrabright Polymer-Dot Transducer Enabled Wireless Glucose Monitoring via a Smartphone. *ACS Nano* **2018**, *12*, 5176–5184.

(23) Chan, Y.-H.; Ye, F.; Gallina, M. E.; Zhang, X.; Jin, Y.; Wu, I.-C.; Chiu, D. T. Hybrid Semiconducting Polymer Dot–quantum Dot with Narrow-Band Emission, near-Infrared Fluorescence, and High Brightness. *J. Am. Chem. Soc.* **2012**, *134*, 7309–7312.

(24) Rong, Y.; Wu, C.; Yu, J.; Zhang, X.; Ye, F.; Zeigler, M.; Gallina, M. E.; Wu, I.-C.; Zhang, Y.; Chan, Y.-H. Multicolor Fluorescent Semiconducting Polymer Dots with Narrow Emissions and High Brightness. *ACS Nano* **2013**, *7*, 376–384.

(25) Wu, C.; Jin, Y.; Schneider, T.; Burnham, D. R.; Smith, P. B.; Chiu, D. T. Ultrabright and Bioorthogonal Labeling of Cellular Targets Using Semiconducting Polymer Dots and Click Chemistry. *Angew. Chemie - Int. Ed.* **2010**, *49*, 9436–9440.

(26) Yu, W. W.; Peng, X. Formation of High-Quality CdS and Other II-VI Semiconductor Nanocrystals in Noncoordinating Solvents: Tunable Reactivity of Monomers. *Angew. Chemie - Int. Ed.* **2002**, *41*, 2368–2371.

(27) Li, J. J.; Wang, Y. A.; Guo, W.; Keay, J. C.; Mishima, T. D.; Johnson, M. B.; Peng, X. Large-Scale Synthesis of Nearly Monodisperse CdSe/CdS Core/Shell Nanocrystals Using Air-Stable Reagents via Successive Ion Layer Adsorption and Reaction. *J. Am. Chem. Soc.* **2003**, *125*, 12567–12575.

(28) Lees, E. E.; Nguyen, T.-L.; Clayton, A. H. A.; Mulvaney, P. The Preparation of Colloidally Stable, Water-Soluble, Biocompatible, Semiconductor Nanocrystals with a Small Hydrodynamic Diameter. *ACS Nano* **2009**, *3*, 1121–1128.

(29) Yu, W. W.; Qu, L.; Guo, W.; Peng, X. Experimental Determination of the Extinction Coefficient of CdTe, CdSe, and CdS Nanocrystals. *Chem. Mater.* **2003**, *15*, 2854–2860.

(30) Filbrun, S. L.; Driskell, J. D. A Fluorescence-Based Method to Directly Quantify Antibodies Immobilized on Gold Nanoparticles. *Analyst* **2016**, *141*, 3851–3857.

(31) Chan, Y.-H.; Ye, F.; Gallina, M. E.; Zhang, X.; Jin, Y.; Wu, I.-C.; Chiu, D. T. Hybrid Semiconducting Polymer Dot–Quantum Dot with Narrow-Band Emission, near-Infrared Fluorescence, and High Brightness. *J. Am. Chem. Soc.* **2012**, *134*, 7309–7312.

(32) Wu, C.; Chiu, D. T. Highly Fluorescent Semiconducting Polymer Dots for Biology and Medicine. *Angew. Chemie - Int. Ed.* **2013**, *52*, 3086–3109.

(33) Zhang, Q.; Haddleton, D. M. World Health Organisation Evaluations of the Joint FAO/WHO Expert Committee on Food Additives (JECFA): Cadmium. http://apps.who.int./food-additives-contaminants-jecfa-database/chemical.aspx?chemID=1376 (accessed April 23, 2019).

(34) Blanco-Canosa, J. B.; Wu, M.; Susumu, K.; Petryayeva, E.; Jennings, T. L.; Dawson, P. E.; Algar, W. R.; Medintz, I. L. Recent Progress in the Bioconjugation of Quantum Dots. *Coord. Chem. Rev.* **2014**, *263*, 101–137.

(35) Creamer, A.; Wood, C. S.; Howes, P. D.; Casey, A.; Cong, S.; Marsh, A. V; Godin, R.; Panidi, J.; Anthopoulos, T. D.; Burgess, C. H. Post-Polymerisation Functionalisation of Conjugated Polymer Backbones and Its Application in Multi-Functional Emissive Nanoparticles. *Nat. Commun.* **2018**, *9*, 3237.

(36) Jasieniak, J.; Smith, L.; van Embden, J.; Mulvaney, P.; Califano, M. Re-Examination of the Size-Dependent Absorption Properties of CdSe Quantum Dots. *J. Phys. Chem. C* **2009**, *113*, 19468–19474.

(37) Uddayasankar, U.; Shergill, R. T.; Krull, U. J. Evaluation of Nanoparticle–Ligand Distributions To Determine Nanoparticle Concentration. *Anal. Chem.* **2015**, *87*, 1297–1305.